Biophysical Journal Volume 65 October 1993 1660–1665

A Photoacoustic Calorimetry Study of Horse Carboxymyoglobin on the 10-Nanosecond Time Scale

Christopher L. Norris and Kevin S. Peters*
Department of Chemistry and Biochemistry, University of Colorado, Boulder, Colorado, USA

ABSTRACT The development of a photoacoustic calorimeter with a time resolution of 10 ns is presented, and the dynamics of the enthalpy and volume changes found in the photodissociation of CO from horse carboxymyoglobin are examined. With this enhanced time resolution a new transient species, the lifetime of which is 29 ns at 20°C, is observed in the ligand dissociation process.

INTRODUCTION

The mechanism for ligand association-dissociation within myoglobin has been extensively investigated (Peters, 1991). Although there is a good description, in terms of structure (Kendrew et al., 1960; Kuriyan et al., 1986; Ringe et al., 1984; Takano, 1977) and energetics (Johnson et al., 1992) for the overall association-dissociation reactions, little is known about the nature of the intermediate states that intervene in the ligand-binding process (Case and Karplus, 1979). Time-resolved spectroscopic techniques allow for the kinetic characterization of transient species (Austin et al., 1975; Henry et al., 1983), but the associated energetics, which are fundamental to the development of an understanding of the ligand-binding process, are exceedingly difficult to ascertain. With the development of time-resolved photoacoustic calorimetry, the dynamics of both enthalpy and volume changes that accompany ligand dissociation can now be discerned (Peters and Snyder, 1988).

In a recent publication we presented the results of a time-resolved photoacoustic calorimetry study of horse carboxymyoglobin (Westrick and Peters, 1990). These experiments measured the dynamics of the enthalpy and volume changes of the protein that accompany the diffusion of carbon monoxide from the heme pocket into the solvent following photolysis. The time resolution of the experiment was 100 ns. We found that within 100 ns photodissociation of carbon monoxide produced an intermediate with an increase of enthalpy of 7.4 ± 2.0 kcal/mol and a decrease in volume of −1.7 ± 0.5 ml/mol relative to carboxymyoglobin in Tris buffer (pH 8.0). The intermediate then decayed in 700 ns at 20°C to produce a new species with an overall increase in enthalpy of 14.3 ± 2.9 kcal/mol and an increase in volume of 13.8 ± 0.7 ml/mol relative to that of carboxymyoglobin. Within the error of the experiment the overall binding enthalpy of CO determined by photoacoustic calorimetry is the same as the binding enthalpy that we have recently determined by thin-layer gas solution microcalorimetry (ΔH = −17.3 ± 0.05 kcal/mol).

In this report we detail the development of a photoacoustic calorimeter with an enhanced time resolution of 10 ns. With this increase in time resolution we have observed a new transient species in the photoinduced CO dissociation from horse carboxymyoglobin, the lifetime of which is 29 ns at 20°C. The enthalpy change associated with the formation of this new species is 10 ± 2.6 kcal/mol, and the accompanying volume change is 0.8 ± 0.6 ml/mol.

EXPERIMENTAL

Materials

Horse skeletal muscle metmyoglobin (Sigma) was dialyzed in 0.10 M Tris-HCl buffer (pH 8.0) prior to use. The samples were filtered through a 0.45-mm Lida syringe filter both before and after dialysis and then were deoxygenated for 2 h with occasional stirring under water-saturated N_2 that was produced by bubbling the gas through a buffer reservoir. A 10-fold molar excess of sodium dithionite was used to reduce the sample, followed by exposure to CO to form carboxymyoglobin. Either metmyoglobin or bromocresol purple (Aldrich) was used as calibration compounds. Both gave photoacoustic waveforms identical to that produced by deoxymyoglobin, which relaxes fully in less than 20 ps (Genberg et al., 1987; Richard et al., 1992), with the exception of a time-shift mismatch due to the difference in the speed of sound from the presence of sodium dithionite in deoxymyoglobin (see Data Analysis). It should be noted, however, that a recent report suggests nanosecond relaxation kinetics exist in metheme compounds such as metmyoglobin (Genberg et al., 1991). Care was taken to ensure that all samples were dissolved in buffers of identical composition and that evaporation during degassing was minimized to avoid differences in the speeds of sound for all solutions used.

Apparatus

A PRA nitrogen-pumped dye laser (LN1000/LN102) (operating at 1.5 Hz, 500 nm, pulsewidth 500 ps, and between 5 and 9 μJ per pulse) was used for excitation. The sample is transferred, using nitrogen gas, into a serum-stoppered cuvette embedded in an aluminum block thermostatted with either a Haake A80 or a Laude RM6 temperature bath controller. A chromel/alumel thermocouple in direct contact with the solution is used to monitor temperature. The light is focused to a thin line (4 mm × 70 μm) with a 15-cm cylindrical lens. This configuration was found to give linear response with respect to acoustic intensity and excitation absorbance at pulse energies up to 10 μJ. The acoustic waves are detected by a polyvinylidene difluoride film (52 μm thickness) and metallized with silver ink coatings (Atochem, Valley

Received for publication 19 April 1993 and in final form 20 July 1993.

Address reprint requests to Dr. Kevin Peters, Department of Chemistry and Biochemistry, Campus Box 215, University of Colorado, Boulder, CO 80309-0215.

0006-3495/93/10/1660/06 $2.00

Forge, PA). This film is housed in a stainless steel casing that is epoxied to the cuvette, with one side of the film in direct contact with the solution being studied. The Tris buffer used was found not to alter the response of the sensor over time. The transducer's output is amplified by a Panametrics 5676 40-dB preamplifier, recorded by a Gould 4072 digital storage oscilloscope at 2.5 ns per interval, and stored on an IBM PC-AT. Laser Precision Rj-7000 pyrolytic energy probes are used to monitor both the laser energy and the transmittance of the solutions to the excitation beam. Typically, 100 laser shots were averaged, although some data sets utilized up to 500 shot signal averages.

Data analysis

The photoacoustic signal magnitude, S, is produced by a volume change, ΔV, arising from the expansion or contraction induced by the excitation. This is due of two possible sources: an enthalpic heat release or uptake, which gives rise to an ensuing expansion or contraction of the solvent molecules about the sample, and an intrinsic volume change within the sample molecule itself. Included in this second source are electrostrictive volume changes caused by the reorganization of solvent molecules about created or buried ionic charges. These two sources, ΔV_{th} and ΔV_{con}, when combined, give rise to the acoustic signal

$$S = K(\Delta V_{th} + \Delta V_{con}) = K[(\beta/C_p\rho)Q + \Delta V_{con}], \quad (1)$$

where Q is the heat released from the excited electronic state produced by the absorption, β is the volume thermal expansion coefficient, C_p is the heat capacity, and ρ is the density of the solution. The parameter K is an instrument response factor. It is eliminated by the use of a calibration compound known to liberate the entire absorbed photon energy as heat on a time scale that is significantly faster than the time resolution of the instrument ($<<10$ ns). Because its acoustic contribution is due purely to the thermally released photon energy, $E_{h\nu}$, its magnitude is given by

$$S_{cal} = K(\beta/C_p\rho)\, E_{h\nu}. \quad (2)$$

Dividing the sample's signal by that of the calibrant gives the amplitude ratio, ϕ, defined as

$$\phi = S/S_{cal} = Q/E_{h\nu} + \Delta V_{con}(C_p\rho/\beta E_{h\nu}). \quad (3)$$

Rearranging gives

$$E_{h\nu}\phi = Q + \Delta V_{con}(C_p\rho/\beta). \quad (4)$$

In aqueous solutions, the term containing the thermal expansion coefficient, $C_p\rho/\beta$, is highly temperature dependent. Thus, by making the implicit assumption that Q and ΔV_{con} are temperature independent over a fairly narrow range of approximately 15°C, correlation of the amplitude ratio, ϕ, with temperature gives ΔV and Q. The enthalpy change with respect to the ground state is then $\Delta H = E_{h\nu} - Q$.

Until now, the discussion has assumed that all acoustic waves have the same temporal shape. However, if reactions take place on a time scale that the transducer can resolve (10 to 1000 ns), it results in a significant change in the shape of the wave. In general, for the same amount of energy released, a delayed reaction produces a wave that is shifted in time and smaller in amplitude than an equivalent instantaneous reaction. Specifically, the acoustic signal, $S(t)$, becomes the convolution of the instrument response function, $T(t)$, and the time-dependent decay curve, $H(t)$:

$$S(t) = T(t) * H(t). \quad (5)$$

The acoustic wave produced by the calibration compound experimentally gives $T(t)$. Assuming a sequence of one instantaneous decay followed by two sequential first-order decays, $H(t)$ is represented as

$$H(t) = \phi_1\delta(t) + (\phi_2/\tau_2)\exp(-t/\tau_2) + [\phi_3/(\tau_2 - \tau_3)][\exp(-t/\tau_2) - \exp(-t/\tau_3)] \quad (6)$$

where $\delta(t)$ is Dirac delta distribution, $\tau_n = 1/k_n$, where k_n is the first-order rate constant for the nth process, and ϕ_n is defined as the ratio of released acoustic energy, $E_n/E_{n,\,cal}$; this change takes into account the effect of delayed decay kinetics on the signal magnitude S, but such that the latter part of Eq. 3 still applies.

Several authors have proposed algorithms for photoacoustic deconvolution that utilize nonlinear least-squares fitting of the data as numerically convoluted in the time domain (Arnaut et al., 1992; Rudzki Small et al., 1992). The methodology of this work is the same; it uses the Grinvald-Steinberg fast convolution algorithm (Demas, 1983) combined with the downhill-simplex method of Nelder and Mead (O'Neill, 1985) to accomplish the multidimensional parameter searching. This combination is found to give good results for up to three decays (one instantaneous, two delayed), provided that the delayed processes have time constants τ of $\geq$10 ns, as the Grinvald-Steinberg algorithm has been shown to fail at short τ values.

In addition to the three ϕ values and two τ values, a time-shift parameter was also varied to allow for optimum time axis alignment of the sample wave with the instrument response. This is necessary because under the current experimental setup, the temperature dependence of the speed of sound allows for fluctuations in acoustic transit time of ±0.6 ns/0.1°C fluctuation in temperature, which is the best tolerance of the temperature controllers used. In addition, there is a systematic increase in the speed of sound of about one part in 2000 for solutions containing 1 mM sodium dithionite, seen in wave comparisons between deoxymyoglobin (which contains dithionite) and the calibrants used. This results in an approximately 1.5-ns systematic offset in the acoustic arrival time for carboxymyoglobin (MbCO) versus that of bromocresol purple or metmyoglobin. (Dithionite reacts with both compounds and thus could not be included in the calibrant solution.) An alternative would involve using deoxymyoglobin as the calibrant; however, its extreme sensitivity to oxygen and carbon monoxide contamination precluded its use in this study, although other studies have successfully utilized it (Westrick et al., 1987). The time shifting was accomplished by parabolic interpolation of the experimental sample wave. This was then compared to the calculated convoluted wave by residuals analysis, and the sum of squares of residuals was minimized to find the optimized parameters.

RESULTS

By carrying out photoacoustic experiments at the null point in the thermal expansion coefficient (3.0°C for 0.1 M Tris buffer) one can obtain the pure conformational volume change signal for MbCO. The resulting data are shown in Fig. 1. For comparison, the shape of the instrument response curve is shown by bromocresol purple at 3.5°C, appropriately shifted in time to account for the temperature dependence of the speed of sound. The acoustic trace for MbCO

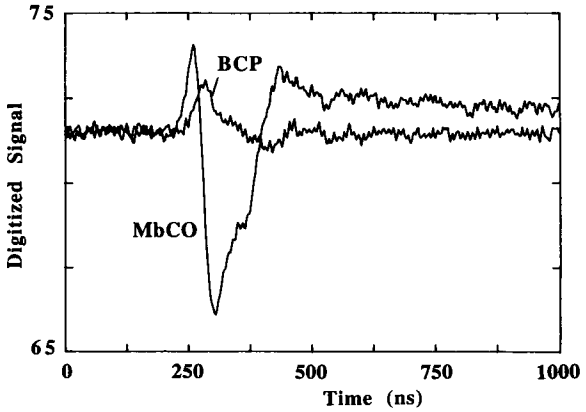

FIGURE 1 Acoustic wave of MbCO at the β-null point of 0.1 M Tris buffer (3.0°C). For waveshape comparison, the wave of the calibrant bromocresol purple (*BCP*) is shown at 3.5°C and is shifted 5 ns later in time to account for the difference in the speed of sound at the two temperatures. Averages of approximately 450 laser shots.

shows a highly unusual shape, revealing the presence of no less than three processes on distinctly different time scales. An immediate positive volume change is followed by a slightly delayed, larger-magnitude negative volume change, which is then followed by a delayed process of positive volume change decaying slowly back to baseline.

The need for a three-decay model is further borne out by experiments near room temperature. The acoustic waves for bromocresol purple and MbCO at 25.6°C are shown in Figs. 2 and 3. The best-fitting result of a simple two-decay model (one instantaneous, one delayed) is shown by the dotted curve in Fig. 2. It shows clear misfitting of the MbCO data, particularly at the peak and the acoustic reflection shoulder that appears at approximately 170 ns on the plot. Adding an additional decay gives the fit in Fig. 3. It shows significantly improved fitting of both the peak and the reflection shoulder and an overall smoother residual curve. The additional decay appears as a negative acoustic event at an intermediate time scale between two positive processes—exactly what would be expected based on the 3.0°C runs of Fig. 1.

The results of all the runs, carried out between 17 and 30°C, are shown in the $E_{h\nu}\phi$ least-squares plots of Fig. 4. The differences in the scattering of the data for the three fits shown can be explained in the following manner. It is primarily the peak of the MbCO wave that determines the values of ϕ_1 and ϕ_2; the accuracy of the individual values are limited by how well the peak can be partitioned into the two components. Thus, there exists a strong anticorrelation between ϕ_1 and ϕ_2; when one is overestimated, the other must be underestimated, and vice versa, in order to conserve the overall peak height. It is for this reason that the $(\phi_1 + \phi_2)$ values show significantly less scatter than the ϕ_1 values alone. (The ϕ_2 values alone show scatter comparable to those of ϕ_1.) Meanwhile, the $\phi_1 + \phi_2 + \phi_3$ data show significant scatter due to the large intrinsic error in ϕ_3, resulting from the small signal-to-noise ratio for the third decay, and thus reveal little regarding the overall enthalpy of CO binding.

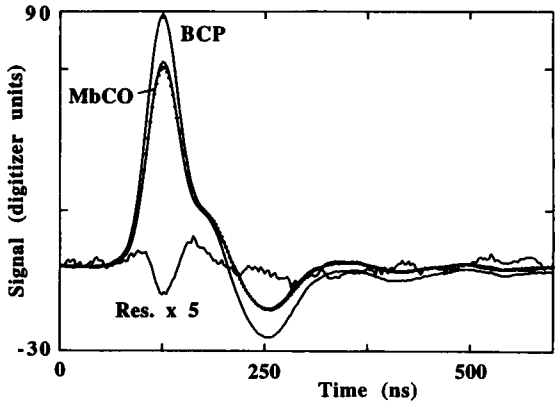

FIGURE 2 Acoustic waves of MbCO and bromocresol purple (*BCP*) at 25.6°C, approximately 100 laser shots averaged. The dotted curve is a calculated best fit for a sequential two-decay model (one instantaneous, one time resolved). Fit parameters: $\phi_1 = 0.767$; $\phi_2 = 0.955$; $\tau_2 = 826$ ns; time shift = 3.27 ns; sum of squares of residuals = 111.8. The residual curve, magnified by a factor of 5 (residuals ×5), is also shown.

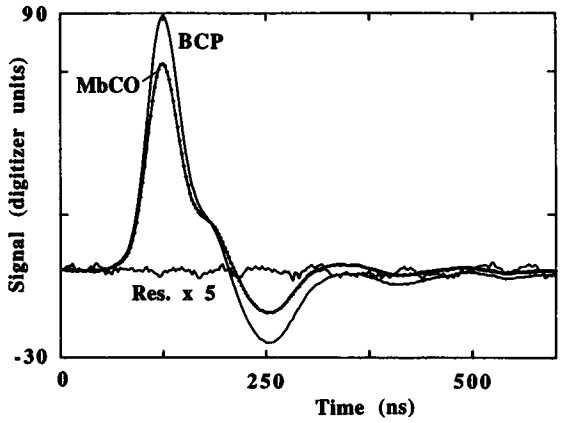

FIGURE 3 As in Fig. 2, except that the dotted curve is a calculated best fit for a sequential three-decay model (one instantaneous, two time resolved), validating the necessity of the third decay. Fit parameters: $\phi_1 = 0.884$; $\phi_2 = -0.125$; $\tau_2 = 16.9$ ns; $\tau_3 = 0.693$; $\tau_3 = 487$ ns; time shift = 1.81 ns; sum of squares of residuals = 16.39.

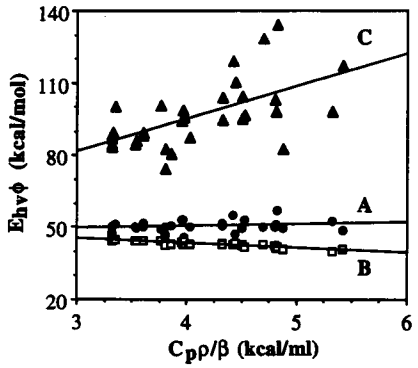

FIGURE 4 Plot of $E_{h\nu}\phi$ versus $C_p\rho/\beta$. The slope of the regression line gives ΔV, and the y-intercept gives Q, the enthalpy released from $E_{h\nu}$ above the MbCO ground state. (*A*) $E_{h\nu}\phi_1$; (*B*) $E_{h\nu}(\phi_1 + \phi_2)$; (*C*) $E_{h\nu}(\phi_1 + \phi_2 + \phi_3)$.

Overall, these results agree well with previous measurements carried out within this group (Westrick and Peters, 1990), using a longer time scale resonant piezoelectric transducer (PZT) as the acoustic sensor. The results of the two experiments are compared in Table 1. It is clear that the two experiments are observing the same processes at longer time scales, as evidenced by the enthalpy and volume change measurements for the second and third intermediate, as well as the agreement in the activation parameters for the final decay. The characteristic times for this slow decay are measured at 700 ns at 20°C for the earlier study versus 750 ± 130 ns for the current one. The faster time resolution for the current study has also revealed the presence of an earlier decay, which occurs with a time constant of 29 ± 3 ns, which could not be resolved by the earlier experiment. It shows that the negative volume change observed within the time resolution of the prior experiment occurs in one distinctly resolved step at this time scale. In addition, the earliest resolved intermediate has an enthalpy change of 10.0 ± 2.6 kcal/mol. An

TABLE 1 Enthalpy changes, volume changes, and activation parameters for photodissociation of CO from horse carboxymyoglobin

	Prior study*	Current study
ΔH_1		10.0 ± 2.6 kcal/mol
ΔH_{1+2}	7.4 ± 2.0 kcal/mol	6.2 ± 0.7 kcal/mol
ΔH_{1+2+3}	14.3 ± 2.9 kcal/mol	16 ± 14 kcal/mol
ΔV_1	—	0.8 ± 0.6 ml/mol
ΔV_{1+2}	−1.7 ± 0.5 ml/mol	−1.91 ± 0.16 ml/mol
ΔV_{1+2+3}	13.8 ± 0.7 ml/mol	13 ± 3 ml/mol
$\Delta H_2^{\ddagger}$	—	8.8 ± 2.0 kcal/mol
$\Delta H_3^{\dagger}$	10.2 ± 0.7 kcal/mol	9.5 ± 1.7 kcal/mol
$\Delta S_2^{\dagger}$	—	6 ± 6 cal/mol K
$\Delta S_3^{\ddagger}$	4.0 ± 2.2 cal/mol K	2 ± 6 cal/mol K

* Westrick and Peters, 1990.

overall enthalpy scheme based upon the present and prior experiments is given in Fig. 5.

The enthalpy change accompanying the formation of the instantaneously produced intermediate species is in accord with the results of Choy and co-workers (Leung et al., 1987), who obtained an enthalpy change following Fe-CO bond cleavage of 13.4 ± 0.5 kcal/mol in 0.1 M phosphate buffer at pH 7. Their method of data analysis differed from ours in that they subtracted the volume change signal obtained at the β-null temperature from their MbCO waves at higher temperature. They then observed that the resulting waves had the same temporal shape as their calibration compound, which meant that the only enthalpy changes that were occurring were prompt. The enthalpy released was measured by the amplitude of this signal. It should be pointed out that this method assumes temperature-independent behavior of the volume-change acoustic signals, which the current study shows may not be the case, since the activation energies for the time-resolved processes are on the order of 9–10 kcal/mol. However, we carried out a similar analysis with our data and found that the volume-subtracted acoustic waves did not have the same temporal shape as the calibration compound. Furthermore, an analogous enthalpy change of $\Delta H = 9 \pm 1$ kcal/mol was determined using this means of data analysis, which is not in statistical agreement with the results of Choy (Leung et al., 1987). The reason for this discrepancy is not clear, but it may be due to the differing buffer conditions for the two experiments. The possibility of proton transfer events occurring at this fast time scale cannot be ruled out, since phosphate and Tris-HCl buffers have vastly different enthalpies of protonation. More experiments must be carried out to account for this possibility.

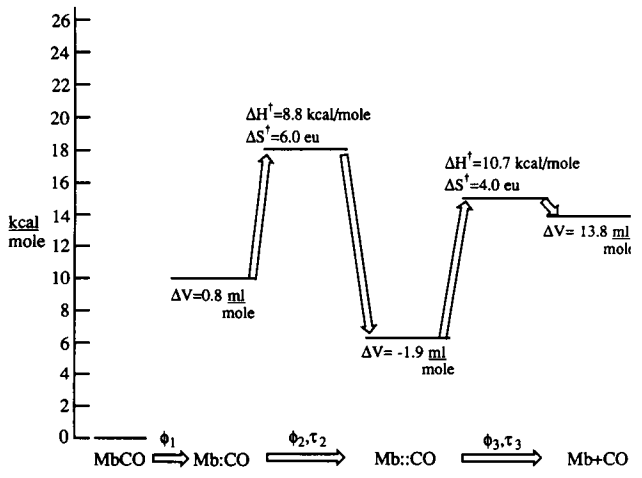

FIGURE 5 Enthalpy scheme for MbCO, 0.1 M Tris buffer (pH 8.0), based on the best compiled data in Table 1.

Picosecond phase grating experiments carried out by Miller and co-workers (Richard et al., 1992) revealed no acoustic processes occurring between 100 ps and several nanoseconds near room temperature. The enthalpy change for the instantaneous process, occurring in less than 20 ps, was measured at 21 ± 2 kcal/mol in a 75% glyerol/water solution. While the kinetics for the two experiments agree, the thermodynamics cannot be directly compared because of the difference in the solvent.

DISCUSSION

The majority of photoacoustic calorimetry experiments have been conducted using lead zirconate-lead titanate PZTs (Peters, 1991). For most applications, the added sensitivity of PZTs over alternative sensors, such as polyvinylidene difluoride, is the main motivating factor for their use. However, the resonant character of most PZTs may preclude their use for certain applications requiring multiexponential fits. Under such resonant conditions, an instrument response wave behaves essentially as a sinusoid; furthermore, any convoluted acoustic wave will also behave as a sinusoid, which is different from the instrument response essentially only because of a phase shift. (In actuality, true resonant acoustic waves deviate slightly from this simplistic sinusoidal picture, but for this qualitative discussion this description suffices.) Sums of sinusoids of the same frequency but with different amplitudes and phases will give net acoustic waves that are also sinusoids at the same frequency. Thus, the shape of the acoustic wave becomes very indifferent to the underlying kinetic components; that information is essentially contained within the phase alone.

Broadband transducers, such as polyvinylidene difluoride, offer an inherent advantage in that they are able to better reflect the true change in shape that occurs in the delayed acoustic wave. This can be seen in Fig. 6, where photoacoustic waves of the same time scales as seen in this study are compared. Each acoustic wave has a shape that is drastically different from the other. When summed together, the net acoustic wave then contains significant information in its shape alone, which can then allow adequate deconvolution of the individual components. In addition, when difficulties such as time-shift artifacts are present, those can be fit for because the kinetic information is not as highly partitioned into the phase of the signal. Such a deconvolution would be significantly more difficult in the case of a resonant transducer.

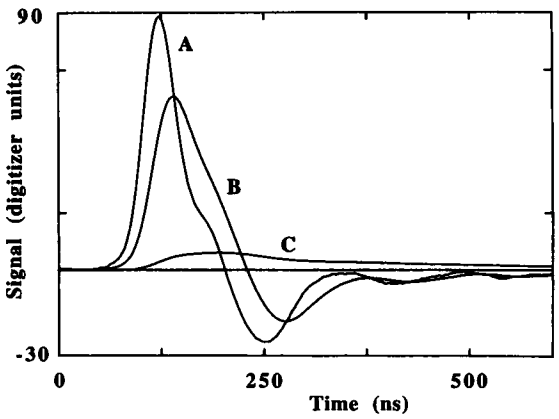

FIGURE 6 Simulated single-decay acoustic waves with the same amplitude ratio ($\phi = 1.0$), showing the drastic change in wave shape as a function of decay time. (*A*) $\tau = 0$ (instantaneous decay); (*B*) $\tau = 29$ ns; (*C*) $\tau = 750$ ns.

The results of prior horse MbCO studies within this group (Westrick and Peters, 1990) were interpreted in terms of a salt bridge solvation model developed from photoacoustic experiments on sperm whale MbCO (Westrick et al., 1987, 1990). X-ray crystal structures of sperm whale deoxymyoglobin reveal that a salt bridge exists between an arginine in the CD loop (Arg45) and a propionate side chain on the heme prosthetic group (Ringe et al., 1984). In sperm whale MbCO, roughly equal populations of open and closed conformations for this salt bridge are found to exist (Kuriyan et al., 1986). X-ray studies conducted with myoglobin ligated to an imidazole (Bolognesci et al., 1982) or a phenyl group (Ringe et al., 1984) show a large displacement of the distal histidine, His-E7, causing the salt bridge to open and revealing a possible path for ligand diffusion between the charges. The present model proposes that in sperm whale MbCO, a significant proportion of the arginine-propionate salt bridges are intact. Upon photodissociation, these bridges open on a time scale of <100 ns, creating the channel for ligand escape. This opening results in solvation of the ionic species, creating electrostriction by the solvent and giving rise to a large negative volume change. Then, on a time scale of 700 ns at 20°C, the salt bridge reforms after ligand escape has occurred, producing a large positive volume change. This model was tested by carrying out experiments on mutant sperm whale MbCO where the Arg-45 was replaced either with asparagine or glycine in order to disrupt the salt bridge. Indeed, the magnitude of the ΔV for the fast (<100 ns) process became significantly less negative compared to the native protein, while the enthalpy change became significantly more positive, presumably reflecting the absence of solvation. However, activation parameters for the 700-ns process were the same in the native and mutant forms, suggesting that salt bridge closure was not the rate-determining step for the process. Additionally, the overall enthalpy and volume changes were also the same, suggesting that there was no net change in the solvation state of the Arg-45 cation between MbCO and the unligated product.

Previous experiments on horse MbCO (Westrick and Peters, 1990), which has a lysine in place of Arg-45, revealed that the volume change of the intermediate produced in <100 ns was even less negative than in the mutated sperm whale, while the enthalpy change was comparable. The overall volume change showed a significantly larger positive ΔV, as did the enthalpy change. This suggested that there was a distinctive change in the degree of solvation about the residue between the initial and final products, which is consistent with the lysine-propionate bridge initially being open and then closing upon ligand escape. That the kinetic and activation parameters of the 700-ns process were almost identical with those of both the native and mutant sperm whale myoglobins further supports this proposal.

Structurally, the 700-ns salt bridge closure event can be interpreted as a change from the A_0 to A_1 conformational structure seen in infrared and resonance Raman studies of sperm whale MbCO, where the A_0 "open" structure corresponds to the distal histidine displaced toward the solvent (Morikis et al., 1989). The time scales for such interconversions are slow and exist primarily on the 10–50-μs time scale in 75% glycerol/water in solution (Tian et al., 1992). However, the time scale could be shortened to 1 μs or less in aqueous solution, given its viscosity dependence.

The interpretation of the 29-ns event is more problematic. Spectroscopic evidence for processes on this time scale have been observed by Champion and co-workers, who attribute the nonexponential rebinding kinetics of sperm whale MbCO at ambient temperatures in aqueous solution to a protein relaxation coupled to an iron-proximal histidine distance change occurring on a time scale of less than 100 ns (Tian et al., 1992). Soret spectral changes in sperm whale MbCO have been observed by Eaton and co-workers on nanosecond to microsecond time scales (Ansari et al., 1992). Similar spectral changes were seen by Boxer in the photodissociation of human MbCO in 75% glycerol/buffer solutions; one component of the kinetic process occurs on the 30-ns time scale (Lambright et al., 1991). It is noted, however, that kinetic comparisons between glycerol solutions and aqueous solutions are difficult to make because of the strong viscosity effects that exist in these systems (Ansari et al., 1992; Beece et al., 1980). Also, comparisons between myoglobins of different species should be viewed with caution.

Because limited structural and kinetic information is available for horse myoglobin, it is important to carry out photoacoustic calorimetric measurements with the current improved time resolution on sperm whale myoglobin. Such experiments can then be compared to the wide range of techniques that have been applied to this widely studied form of myoglobin. Currently, there is little agreement on the kinetic parameters for processes obtained using various biophysical techniques; this is not surprising considering that each technique monitors processes that occur by different means and barriers of differing natures. Experiments (Austin et al., 1975) suggest that ligand diffusion should occur as a many-barrier process, and no single technique will be expected to have the capacity to monitor all of them. Compilation of data

using all techniques should be able to provide a more unified model of the ligand diffusion process.

This work was supported by a grant from the National Science Foundation (DMB 9004667).

REFERENCES

Ansari, A., C. M. Jones, E. R. Henry, J. Hofrichter, and W. A. Eaton. 1992. Role of solvent viscosity in the dynamics of protein conformational changes. *Science (Washington DC).* 256:1796–1798.

Arnaut, L. G., R. A. Caldwell, J. E. Elbert, and L. A. Melton. 1992. Recent advances in photoacoustic calorimetry: theoretical basis and improvements in experimental design. *Rev. Sci. Instrum.* 63:5381–5389.

Austin, R. H., K. W. Beeson, L. Eisenstein, H. Frauenfelder, and I. C. Gunsalus. 1975. Dynamics of ligand binding to myoglobin. *Biochemistry.* 14:5355–5373.

Beece, D., L. Eisenstein, H. Frauenfelder, D. Good, M. C. Marden, L. Reinisch, A. H. Reynolds, L. B. Sorensen, and K. T. Yue. 1980. Solvent viscosity and protein dynamics. *Biochemistry.* 19:5147–5157.

Bolognesci, M., E. Cannillo, P. Ascenzi, G. M. Giacometti, A. Merli, and M. Brunori. 1982. Reactivity of ferric *Aplysia* and sperm whale myoglobins towards imidazole. *J. Mol. Biol.* 158:305–315.

Case, D. A., and M. Karplus. 1979. Dynamics of ligand binding to heme proteins. *J. Mol. Biol.* 132:343–368.

Demas, J. N. 1983. Excited State Lifetime Measurements. Academic Press, New York.

Genberg, L., F. Heisel, G. McLendon, and R. J. D. Miller. 1987. Vibrational energy relaxation processes in heme proteins: model systems of vibrational energy dispersion in disordered systems. *J. Phys. Chem.* 91:5521–5524.

Genberg, L., L. Richard, G. McLendon, and R. J. D. Miller. 1991. Direct observation of global protein motion in hemoglobin and myoglobin on picosecond time scales. *Science (Washington DC).* 251:1051–1054.

Henry, E. R., J. H. Sommer, J. Hofrichter, and W. Eaton. 1983. Geminate recombination of carbon monoxide to myoglobin. *J. Mol. Biol.* 166:443–451.

Johnson, C. R., S. J. Gill, and K. S. Peters. 1992. Thin-layer microcalorimetric studies of oxygen and carbon monoxide binding to hemoglobin and myoglobin. *Biophys. Chem.* 45:7–15.

Kendrew, J. C., R. E. Dickerson, B. E. Strandberg, R. G. Hart, D. R. Davies, D. C. Phillips, and V. C. Shore. 1960. Structure of myoglobin. *Nature (Lond.).* 185:422–427.

Kuriyan, J., S. Wilz, M. Karplus, and G. A. Petsko. 1986. X-ray structure and refinement of carbonmonoxy (FeII) myoglobin at 1.5 Å resolution. 1986. *J. Mol. Biol.* 192:133–154.

Lambright, D. G., S. Balasubramanian, and S. G. Boxer. 1991. Protein relaxation dynamics in human myoglobin. *Chem. Phys.* 158:249–260.

Leung, W. P., K. C. Cho, S. K. Chau, and C. L. Choy. 1987. Measurement of the protein-ligand bond energy of carboxymyoglobin by pulsed photoacoustic calorimetry. *Chem. Phys. Lett.* 141:220–224.

Morikis, D., P. M. Champion, B. A. Springer, and S. G. Sligar. 1989. Resonance Raman investigations of site-directed mutants of myoglobin: effects of distal histidine replacement. *Biochemistry.* 28:4791–4800

O'Neill, R. 1985. Function minimization using a simplex procedure. *In* Applied Statistics Algorithms. P. Griffiths and I. D. Hill, editors. Ellis Horwood, Ltd., London. 78–87.

Peters, K. S.. 1991. Time resolved photoacoustic calorimetry: a study of myoglobin and rhodopsin. *Annu. Rev. Biophys. Biophys. Chem.* 20:343–362.

Peters, K. S., and G. Snyder. 1988. Time-resolved photoacoustic calorimetry: probing the energetics and dynamics of fast chemical and biochemical reactions. *Science (Washington DC).* 241:1053–1057.

Richard, L., L. Genberg, J. Deak, H. L. Chiu, and R. J. D. Miller. 1992. Picosecond phase grating spectrosocopy of hemoglobin and myoglobin: energetics and dynamics of global protein motion. *Biochemistry.* 31:10703–10715.

Ringe, D., G. A. Petsko, D. E. Kerr, and P. R. Ortiz de Montellano. 1984. Reaction of myoglobin with phenylhydrazine: a molecular doorstop. *Biochemistry.* 23:2–4.

Rudzki Small, J., L. J. Libertini, and E. W. Small. 1992. Analysis of photoacoustic waveforms using nonlinear least squares method. *Biophys. Chem.* 42:29–48.

Takano, T. 1977. Structure of myoglobin refined at 2.0 Å resolution. *J. Mol. Biol.* 110:537–584.

Tian, W. D., J. T. Sage, V. Srajer, and P. M. Champion. 1992. Relaxation dynamics of myoglobin in solution. *Phys. Rev. Lett.* 68:408–411.

Westrick, J. A., and K. S. Peters. 1990. A photoacoustic calorimetry study of horse myoglobin. *Biophys. Chem.* 37:73–79.

Westrick, J. A., J. L. Goodman, and K. S. Peters. 1987. A time-resolved photoacoustic calorimetry study of the dynamics of enthalpy and volume changes produced in the photodissociation of carbon monoxide from sperm whale carboxymyoglobin. *Biochemistry.* 26:8313–8318.

Westrick, J. A., K. S. Peters, J. D. Ropp, and S. G. Sligar. 1990. Role of the arginine-45 salt bridge in ligand dissociation from sperm whale carboxymyoglobin as probed by photoacoustic calorimetry. *Biochemistry.* 29: 6741–6746.